Polariton Theory of Raman Scattering. III. Effect of Exciton and Band Properties on the Frequency Dependence of the Cross Section

Bernard Bendow*
Department of Physics, University of California, San Diego, La Jolla, California 92037
(Received 22 February 1971)

In the present work, a polariton approach is employed to derive cross sections for resonant Raman scattering mediated by dipole-forbidden and quadrupole-allowed excitons. The results are contrasted with those in the dipole-allowed case. We investigate differences in polariton dispersion and in the nature of the discrete-state and continuum contributions in the various cases, and demonstrate how these influence the resonance properties of the cross section. We find that, in general, continuum effects dominate in forbidden scattering, while continuum-discrete interference is strongest in allowed scattering. Considerably sharper onsets to resonance are predicted for the quadrupole case, as compared to the dipole. Resonance properties are shown to depend as well, often strongly, on the values of various crystalline parameters, such as the exciton effective mass and the frequency of the phonons involved in the scattering. The predictions are illustrated via detailed numerical computations for a hydrogenic exciton model, and parameters appropriate to insulators such as CdS.

I. INTRODUCTION

At optical frequencies, Raman scattering[1-3] (RS) in insulators and semiconductors proceeds via the scattering of photon-exciton polaritons[4] (composite quasiparticles) by phonons (cf. Fig. 1). As will be demonstrated here, the properties of the cross section depend strongly on the properties of the crystalline states mediating the scattering. We note that dependences of this nature have in fact been investigated in considerable detail for a variety of other effects, such as optical absorption in semiconductors,[5] for example.

The theory of RS by LO phonons has been recently advanced in a number of places.[1-3,6] The most detailed discussions[7] of the frequency dependence of the cross section seem to have been limited to first-order RS (RS1) mediated by dipole-allowed free-exciton transitions. For example, numerical computations for the latter case,[3] within a hydrogenic model, have been presented for the A-exciton in CdS. The purpose of the present paper is the extension and application of the polariton theory of RS1 to an investigation of the dependence of the cross section on the character of the Bloch functions and exciton wave functions[8] involved in the scattering process. Evidently, the variety of such dependences is quite extensive; we here limit our attention to a number of particular cases which, we feel, are of special interest. Among these are (a) dependence of the cross section on the relative sizes of the exciton effective mass, the background dielectric constant, the exciton bandwidth, the phonon frequency, and the ratio of continuum-to-discrete coupling strengths; (b) differences in frequency dependence for "dipole-allowed," "dipole-forbidden," and "quadrupole" transitions.

In our nomenclature, a "dipole" transition proceeds whenever the dipole matrix element $(\vec{p})_{n0}$ is large enough compared to the quadrupole one $(\vec{r}\circ\vec{p})_{n0}$ such that the latter's contribution is negligible; should the reverse be true, e.g., should $(\vec{p})_{n0}$ vanish and $(\vec{r}\circ\vec{p})_{n0}$ not, we then speak of a "quadrupole" transition. "Allowed" and "forbidden" transitions[9] depend also on exciton symmetry properties: Allowed transitions correspond to exciton relative-motion wave function $U(\vec{\beta}=0)\neq 0$, where $\vec{\beta}$ is the relative-motion coordinate; (first) forbidden transitions correspond to $U(0)=0$, while $[\partial U(\vec{\beta})/\partial\vec{\beta}]_0\neq 0$. For a more detailed theoretical account of the various possible transitions under discussion here the reader is directed to Ref. 10. We note in passing some isolated actual examples[11] in Cu_2O: The "1s yellow" line is believed to be a

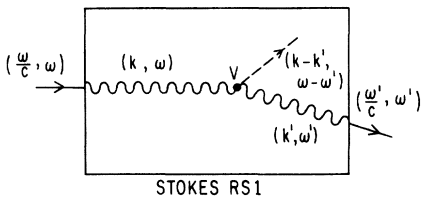

FIG. 1. Schematic of Stokes RS1 scattering by polaritons. An incident photon with (wave vector, frequency) $=(\omega/c,\ \omega)$, represented by a straight line, excites a polariton $(k,\ \omega)$ in the crystal, represented by a wavy line. The polariton scatters via the interaction V, producing a phonon $(k-k',\ \omega-\omega')$, represented by a dashed line. The scattered polariton $(k',\ \omega')$ finally emerges as the photon $(\omega'/c,\ \omega')$.

quadrupole transition, while an entire "green" series is considered to arise via forbidden transitions.

We here adopt the formulation of RS theory detailed in previous papers in this series (Refs. 2 and 3, henceforth referred to as I and II, respectively). We proceed to summarize various results for RS1 obtained there, adopting these results (with appropriate modifications) to specific cases of interest here.

II. FIRST-ORDER RAMAN CROSS SECTION

In this section, we review certain fundamentals of polariton RS, and specify various details of the model to be employed in computations throughout this paper.

Following I and II, the differential cross section for first-order Stokes RS at 0 °K of a polariton $(\vec{q}\omega)$ to a polariton $(\vec{q}'\omega')$ with the production of a phonon $\omega_0 = \omega - \omega'$ is given by ($\hbar, c = 1$):

$$\frac{d\sigma}{d\Omega} = (2\pi)^{-2} q'^2 v_g^{-1}(\vec{q}\omega) v_g^{-1}(\vec{q}'\omega') \left| \sum_{nn'} g^{(3)}_{nn'}(\vec{q}\vec{q}') \times [\chi_n^*(\vec{q}\omega)\chi_{n'}(\vec{q}'\omega') + \phi_n^*(\vec{q}\omega)\phi_{n'}(\vec{q}'\omega')] \right|^2, \quad (1)$$

where the q's are wave vectors and ω's frequencies, and where, for dispersionless dipole excitons, e.g.,

$$\chi_n = (\omega - E_n)^{-1} g_n^* q^{-1/2} v_g^{1/2}(\vec{q}\omega),$$
$$\phi_n = -(\omega + E_n)^{-1} g_n q^{-1/2} v_g^{1/2}(\vec{q}\omega), \quad (2)$$

where E_n and g_n are the exciton energies and (bilinear) couplings to light, $v_g(\vec{q}\omega) \equiv \partial\omega(\vec{q})/\partial\vec{q}$ is the polariton group velocity, and $g^{(3)}_{nn'}$ is the trilinear phonon-exciton coupling function[6] for scattering of exciton n to n'. In general, the sums run over both discrete and continuous indices characterizing the excitons involved. The (χ, ϕ) are polariton transformation coefficients[1-4] relating polaritons to bare excitons. This result is appropriate for the case where a single polariton dominates in both the incoming and outgoing channels. The relationship between $\vec{q}$ and ω is given via the dielectric function $\epsilon(\vec{q}\omega)$ as

$$\epsilon(\vec{q}\omega) \equiv q^2/\omega^2 = \epsilon_0 + \sum_n 4|g_n|^2 E_n^{-1}(E_n^2 - \omega^2)^{-1}, \quad (3)$$

where ϵ_0 is the background dielectric constant.

The Stokes and anti-Stokes (RS1) cross sections for $T > 0$ °K are given by expressions of the form in Eq. (1) multiplied by appropriate phonon occupancy factors. For simplicity we therefore may restrict our considerations to the $T = 0$ °K Stokes result alone.

The results given above have entirely neglected polariton damping[12] in both the incoming and outgoing channels. It is useful to distinguish between two interrelated effects of such damping. First, when damping is present, one expects a distribution of scattered frequencies,[3,13] rather than just energy-conserving scattering restricted to $\omega - \omega' = \omega_0$ (for Stokes RS1). The theory of the associated line shape is discussed in some detail in II. We note, however, that although the cross section adopted above is appropriate only in the energy-conserving limit, it nevertheless does encompass the full range of resonance behavior which is of interest in the present treatment.

A second effect of damping is the broadening of the exciton levels of the system, which causes the incoming and outgoing polaritons to be damped quasiparticles. As demonstrated in the Appendix, even in the limit of energy-conserving transitions, damping effects are non-negligible in a small frequency region (of width of the order of the damping function Γ) about the various exciton-induced resonances and antiresonances. In the Appendix, we demonstrate how a phenomenological approach may be employed to investigate this latter effect of damping on the scattering cross section.

In order to facilitate actual calculations, we now introduce various specializations in parallel with II: (a) We take $g^{(3)}_{nn'}(\vec{q}, \vec{q}') \approx \delta_{nn'} g^{(3)}$, where $g^{(3)}$ is an appropriate constant; and (b) we consider the approximation of nearly dispersionless levels $E_n(\vec{q}) \approx E_n$. These limitations are useful in reducing the present problem to a form best suited for numerical computation, especially when both discrete and continuum levels are included. However, since neither spatial dispersion[2,14] nor polariton damping have been included, special care must be taken in interpreting the predictions of the theory in the resonance regime. Specifically, as discussed in the Appendix, the presence of damping is expected to remove singular behavior and regions of perfect reflection (where an absence of scattering would be predicted) from the cross section.

We will employ a hydrogenic series of levels composed of discrete states $E_n (n = 1, 2, \ldots, \infty)$, and a continuum E_η from the energy gap E_g up to the maximum energy[15] E_M; we then have

$$E_n = E_g - R/n^2, \quad R \equiv e^4/2\alpha_R \epsilon_0^2,$$
$$E_\eta = E_g + \tfrac{1}{2}\alpha_R \eta^2, \quad (4)$$

where R is the exciton Rydberg, α_R is the inverse electron-hole reduced mass $(m_e^{-1} + m_h^{-1})$, and η is the relative-motion wave vector. As mentioned above, we omit the c.m. term $\frac{1}{2}\alpha q^2$, an approximation best suited for the case $\alpha^{-1} \equiv (m_e + m_h) \gg \alpha_R^{-1}$.

For a hydrogenic series, dipole-allowed transitions are described by[9] ($a_0 \equiv$ exciton Bohr radius)

$$g_n = g_1/n^{3/2},$$
$$g_\eta = g_1 \pi (2a_0^3)^{1/2} \gamma_\eta^{1/4} [1 - \exp(-2\pi\gamma_\eta^{1/2})]^{-1/2}, \quad (5)$$

where

$$\gamma_\eta \equiv 2R/\alpha_R \eta^2 . \tag{6}$$

Employing Eqs. (1) and (2) and the above approximations, one obtains the RS1 cross section for dipole-mediated scattering as

$$\left(\frac{d\sigma}{d\Omega}\right)_D = (2\pi)^{-2}\left(\frac{q'}{q}\right)|T_D+T_C|^2|g^{(3)}|^2, \tag{7}$$

where T_D is the discrete-state sum

$$T_D=\sum_n 4|g_n|^2(\omega\omega'+E_n^2)(\omega^2-E_n^2)^{-1}(\omega'^2-E_n^2)^{-1}, \tag{8}$$

and where T_C has the same form as T_D, but where the sum runs instead over the continuum states $\vec{\eta}$. As discussed in detail in II, both the frequency variations of q'/q and $|T_D+T_C|$ significantly influence the frequency dependence of $d\sigma/d\Omega$; in particular, one finds that interference between T_D and T_C exerts an important influence on the resonance behavior. These properties will be evident in the various computations to be presented in Secs. III–V.

III. QUADRUPOLE-TRANSITION RAMAN SCATTERING

In this section, we investigate the frequency dependence of the RS cross section in the quadrupole case, for a hypothetical model of a full series (discrete plus continuous) of exciton levels. The quadrupole case obtains when the first nonvanishing terms in the matrix elements are linear in the wave vector, i.e.,

$$g_{n,\vec{\eta}}(\vec{q}) = q f_{n,\vec{\eta}} g_1 , \tag{9}$$

where, e.g., $f_n = n^{-3/2}$ for allowed transitions, etc. The dielectric function is obtained upon substituting the above $g_{n,\vec{\eta}}(\vec{q})$ into Eq. (3). One then finds the polariton dispersion relation $\omega = \omega(\vec{q})$ has a shape nearly similar to the corresponding dipole result (cf. Ref. 4), differing only in the disposition of the splittings near the discrete exciton frequencies. This is illustrated for a single discrete level, for the parameters indicated, in Fig. 2. The results are meaningful everywhere except for a very small region about the E_n where q becomes very large, and Eq. (9) is inaccurate. A central distinguishing characteristic of the quadrupole dispersion is seen to be a shift downward of the large-q asymptote as compared with the dipole case.

Obtaining the polariton coefficients (χ, ϕ) via the methods of II, one has, after some algebra,

$$\chi_{n,\vec{\eta}} = (\omega - E_{n,\vec{\eta}})^{-1} g^*_{n,\vec{\eta}} q^{-1/2} v_g^{1/2}(\vec{q}\omega)\epsilon^{1/2}(\vec{q}\omega),$$
$$\phi_{n,\vec{\eta}} = -(\omega + E_{n,\vec{\eta}})^{-1} g_{n,\vec{\eta}} q^{-1/2} v_g^{1/2}(\vec{q}\omega)\epsilon^{1/2}(\vec{q}\omega). \tag{10}$$

Incorporating these results, and the previously specified approximations, one obtains the quadrupole RS1 cross section as

$$\left(\frac{d\sigma}{d\Omega}\right)_Q = (2\pi)^{-2}\left(\frac{q'}{q}\right)|T_D+T_C|^2|g^{(3)}|^2 F(q,q'), \tag{11}$$

where T_D and T_C were defined in Sec. II, and where

$$F(q,q') \equiv q^2 q'^2 \epsilon(\vec{q}\omega)\epsilon(\vec{q}'\omega'). \tag{12}$$

Comparison with Eqs. (7) and (8) indicates that $(d\sigma/d\Omega)_Q$ is related to a hypothetical dipole cross section $(d\sigma/d\Omega)_D$ of strength g_1 $[=g_1(q)/q]$ as

$$\left(\frac{d\sigma}{d\Omega}\right)_Q = \left(\frac{d\sigma}{d\Omega}\right)_D F(q,q'). \tag{13}$$

When q and q' lie outside the resonance regime, $F(q,q') \approx q^2 q'^2$, and $(d\sigma/d\Omega)_Q$ reduces, as expected, to the form which would be obtained in the bare exciton approach[6,15] by just replacing $g \to g \times q$ directly into the dipole cross section. However, the present polariton analysis indicates that the actual variation in the resonance regime is $\sim q^4 q'^4$ × (dipole result). Consequently, damping effects being sufficiently small, one expects quadrupole resonances to be much sharper (more abrupt) than dipole ones.

The quadrupole-to-dipole shape ratio $F(q,q')$ is illustrated as a function of incident photon frequency, for a single discrete level E_1, in Fig. 3.

IV. FORBIDDEN-TRANSITION RAMAN SCATTERING

In this section, we derive the cross section for RS mediated by forbidden transitions, and compare with dipole results.

While in the allowed case the coefficients g_n are proportional to $U_{n,\vec{\eta}}(0)$, in the (first) forbidden case[9] they are, instead, proportional to $[\partial U_{n,\vec{\eta}}(\vec{\beta})/\partial\vec{\beta}]_{\vec{\beta}=0}$. For the hydrogenic case, one has

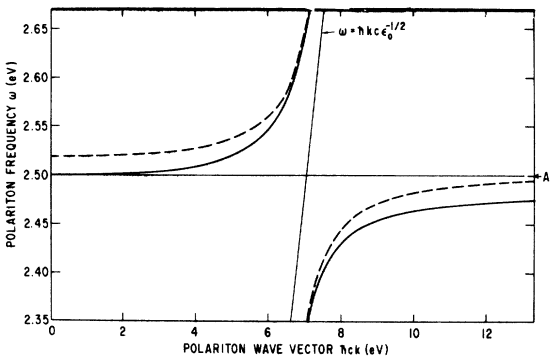

FIG. 2. Dipole and quadrupole polariton frequencies ω vs wave vector $\hbar ck$, for a single level with $E = 2.50$ eV, $|g|^2 = 0.75$ eV^3, and $\epsilon_0 = 8$. Broken line: dipole; solid line: quadrupole. "A" indicates the energy level E.

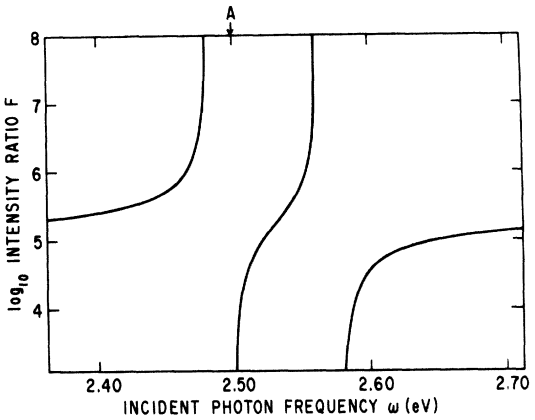

FIG. 3. Log_{10} of the quadrupole-to-dipole intensity ratio F vs incident photon frequency ω. Here $\omega_0 = 0.08$ eV; other parameters are the same as those employed in Fig. 2.

$$\left|\left(\frac{\partial U_n}{\partial \vec{\beta}}\right)_0\right|^2 = \frac{1-n^{-2}}{3a_0^2}\,|U_n(0)|^2\,,$$
$$\left|\left(\frac{\partial U_{\vec{\eta}}}{\partial \vec{\beta}}\right)_0\right|^2 = \frac{1}{3}\left(\frac{2R}{\alpha_R}+\eta^2\right)|U_{\vec{\eta}}(0)|^2, \tag{14}$$

so that the g_n may be written in terms of some single parameter g_1 as

$$|g_n|^2 = [(n^2-1)/n^5]\,|g_1|^2,$$
$$|g_{\vec{\eta}}|^2 = 2\pi^2 a_0^5 \gamma_{\vec{\eta}}^{1/2}\,(1-e^{-2\pi\gamma_{\vec{\eta}}^{1/2}})^{-1}\eta^2(1+\gamma_{\vec{\eta}})\,|g_1|^2\,. \tag{15}$$

To obtain the polariton dispersion and the RS cross section one employs these expressions for $g_{n,\vec{\eta}}$ directly in Eqs. (1)–(3).

Comparing the forbidden cross section $(d\sigma/d\Omega)_F$ obtained in this way with the allowed result $(d\sigma/d\Omega)_A$, one notes that the discrete-state contributions to resonance behavior are identical in shape in the two cases, differing only in the relative intensities within the exciton series, which is $\sim (n/n')^6$ for the allowed case, but $\sim [(n'^2-1)/(n^2-1)]^2\,(n/n')^{10}$ for the forbidden (with the $n=1$ line now absent). The fundamental difference in the frequency dependence of the cross sections arises from differences in $g_{\vec{\eta}}$ and, consequently, the continuum contribution, in the two cases. This is best understood via the relations expressed in Eq. (14). Typically, $(2R/\alpha_R)/a_0^{-2} > 1$, so that the continuum contribution is relatively more important in the forbidden case than the allowed (this is illustrated more explicitly by the computations of Sec. V). For CdS parameters,[16] e.g., this ratio would be $\sim \frac{3}{2}$. Of course, the absence of the $n=1$ level, with its large oscillator strength, also serves to magnify the continuum effect in the cross section.

We have so far considered only the shapes of the two cross sections; as for their relative intensities, following the discussion of Ref. 17, say, one notes that the actual ratio of g_1 in the forbidden case to g_1 in the allowed goes as a/a_0, where a is the lattice constant and a_0 the exciton Bohr radius (cf. Ref. 6). Consequently, the ratio $(d\sigma/d\Omega)_F/(d\sigma/d\Omega)_A \sim (a/a_0)^4$, which for CdS parameters are $\sim 6\times10^{-4}$. Thus intensities of forbidden RS1 are, in general, expected to be smaller than corresponding allowed intensities by at least a few orders of magnitude.

Figure 4 illustrates the frequency dependence of $(d\sigma/d\Omega)_A$ and $(d\sigma/d\Omega)_F$ for CdS parameters (the relative intensity between the two is, however, chosen arbitrarily and is of no significance). Here, as in all cross-section computations to follow, we collapse all levels with $n \geq 3$ onto E_g, as it is impractical and unnecessary to demonstrate the frequency variation associated with such closely spaced levels. The above mentioned domination of continuum effects in $(d\sigma/d\Omega)_F$ is evidenced in Fig. 4 by the extended nearly flat portions of the curves; e.g., the broad antiresonance behavior (due to continuum-discrete state interference) of $(d\sigma/d\Omega)_A$ prior to levelling off at high frequencies, is absent in $(d\sigma/d\Omega)_F$ (for the chosen parameters). For $(d\sigma/d\Omega)_F$, the intensity is nearly similar on both the high- and low-frequency sides of the resonance regions, while for $(d\sigma/d\Omega)_A$ the high-frequency side is substantially depressed.

In Sec. V, the detailed dependence of $(d\sigma/d\Omega)_F$

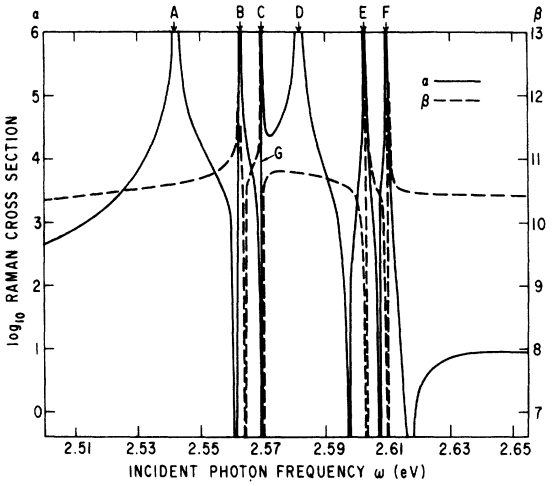

FIG. 4. Log_{10} of the allowed-exciton and forbidden-exciton cross sections vs incident photon frequency ω, for "CdS parameters": $\epsilon_0 = 8$, $\alpha_R^{-1} = 4.3\times10^5$, $g_1 = 0.2$, $E_g = 2.57$, $E_M = 2E_g$, $\omega_0 = 0.04$, $R = 0.028$ (all in eV units, as employed in II, e.g.). Solid line: allowed; broken line: forbidden. A–C indicate E_1, E_2, E_g; D–F the same plus ω_0. A broken line parallel to the solid one at G is omitted to preserve the clarity of the figure.

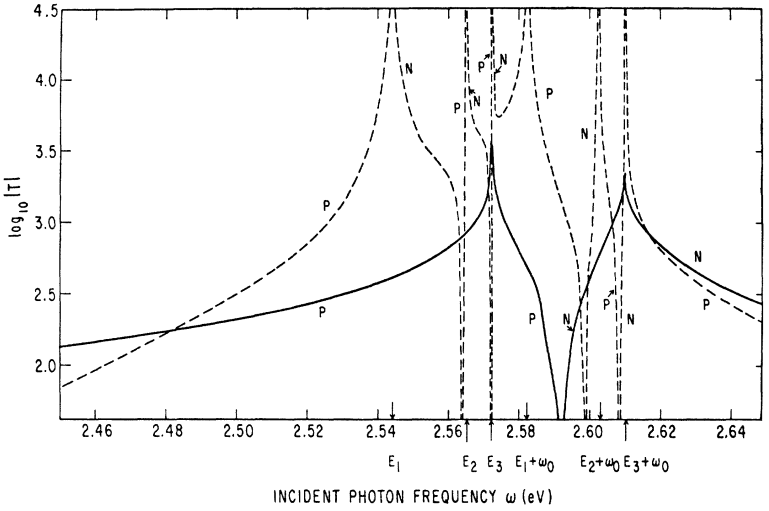

FIG. 5. Log_{10} of $|T_D|$ and $|T_C|$, (discrete-state and continuum contributions to the allowed exciton Raman tensor) vs photon frequency ω (CdS parameters). Solid line: T_C; broken line: T_D. This figure is taken from II, where the slightly different values $\omega_0 = 0.038$ and $E_g = 2.572$ were employed. "P" indicates portions of the curves where T's are positive, and "N" where they are negative.

on various system parameters will be investigated, and comparison with the corresponding $(d\sigma/d\Omega)_A$ carried out.

V. DEPENDENCE OF $d\sigma/d\Omega$ ON VARIOUS SYSTEM PARAMETERS

In this section, we investigate changes induced in the frequency dependence of $(d\sigma/d\Omega)_A$ and $(d\sigma/d\Omega)_F$, when certain of the fundamental crystalline parameters are varied. Specifically, we consider variations in the background dielectric constant ϵ_0, effective mass α_R^{-1}, bandwidth E_M, continuum-to-discrete coupling ratio g_c/g_1, and phonon frequency ω_0.

In the hydrogenic model, if $\alpha_R \to \alpha_R'$ and $\epsilon_0 \to \epsilon_0'$, then[6]

$$R'/R = (\epsilon_0^2/\epsilon_0'^2)(\alpha_R/\alpha_R'), \qquad a_0'/a_0 = (\epsilon_0'/\epsilon_0)(\alpha_R'/\alpha_R), \text{ etc.}, \tag{16}$$

where R is the Rydberg (cf. Sec. II). The energy-level spacings, and the value of the continuum functions $g_{\vec{\eta}}$, depend on the value of R. All of these dependences influence the form of the polariton dispersion, which depends directly on ϵ_0 as well. These then are the principal ways in which changes in α_R and ϵ_0 induce changes in $d\sigma/d\Omega$.

The value of E_M, which appears as a cutoff on the sums (i.e., the integrals) over $\vec{\eta}$ in Eqs. (3) and (7), helps determine the size of the continuum contributions to $d\sigma/d\Omega$. As for the continuum-to-discrete coupling ratio g_c/g_1, this quantity is fixed once a hydrogenic model has been specified. In order to consider more general continuum effects (nonhydrogenic cases, say), we also consider variation in g_c/g_1 in what follows. Turning to the phonon frequency ω_0, its value determines the relative positions of the energy gap and the incoming and outgoing resonances ($\omega, \omega' \sim E_n$), and thereby the resonance properties of the cross section.

The coupling constants g_n may also depend in a variety of ways on the above parameters. Rather than attempt to account for the multiplicity of such dependences,[6,18] we compute $d\sigma/d\Omega$ for fixed values of the g_n in what follows.

We employ the zero-damping theory, as reviewed in Sec. II, for the computations to be carried out in this section. As an aid in generalizing the interpretation of the present results to the case of nonvanishing damping, a phenomenological theory of damped-polariton scattering is presented in the Appendix.

Prior to investigating the frequency dependence exhibited by the full cross section, it is instructive to direct one's attention to the frequency variations of T_D and T_C, as illustrated in Figs. 5 and 6, for allowed and forbidden cases (CdS parameters). From the figures, one easily observes how regions of opposite sign (and opposite sign crossings of the curves) will influence resonance and antireso-

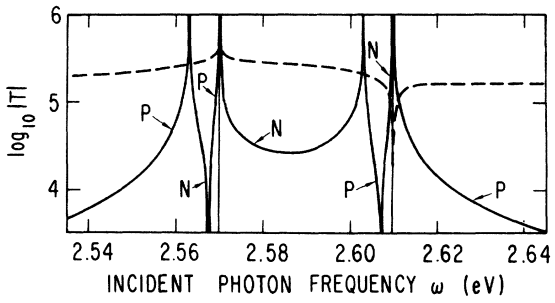

FIG. 6. Log_{10} of $|T_D|$ and $|T_C|$ vs photon frequency ω for the forbidden case (CdS parameters). Solid line: T_D; broken line: T_C. See, for example, Fig. 5 for meanings of various symbols. T_C is here positive everywhere.

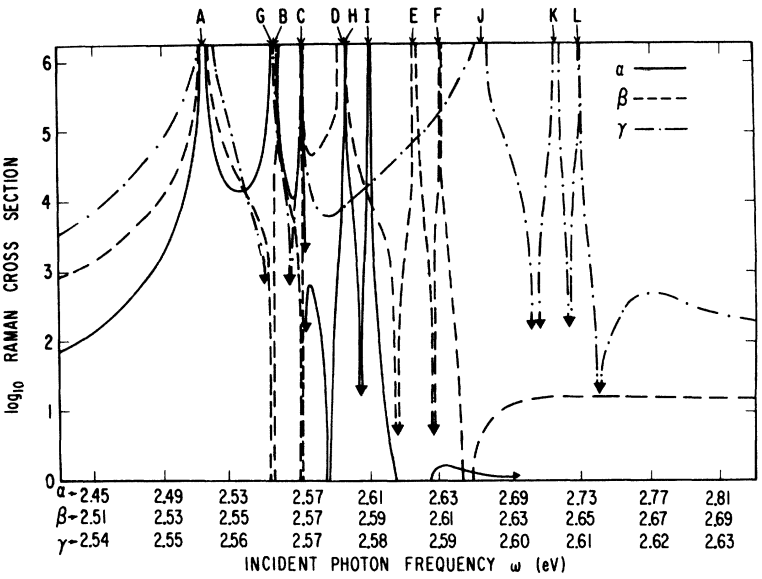

FIG. 7. Log_{10} of allowed cross section vs photon frequency ω for various values of α_R. Dashed line: $\alpha_R = (\alpha_R)_0$ (CdS value); solid line: $\alpha_R = \frac{1}{2}(\alpha_R)_0$; dashed-dot line: $\alpha_R = 2(\alpha_R)_0$. A–C indicate E_1, E_2, E_g; D–F indicate these plus ω_0 for CdS parameters; G–I indicate the same for $\alpha_R = \frac{1}{2}(\alpha_R)_0$; and J–L the same for $\alpha_R = 2(\alpha_R)_0$. A dashed-dot line nearly coincident with the vertical dashed line at B is omitted for clarity. Arrows indicate extensions of the curves in the direction in which they point; they are employed to help unclutter the figures.

nance behavior. For the particular parameters in the figure, the form of $g_{\vec{\eta}}$ leads to positive T_C throughout [cf. Eq. (5)], in contrast to the alternating sign of the allowed contribution. Actually, for large enough α_R and ϵ_0, it can be shown that regions of alternating sign do eventually emerge; however, for present values of parameters this will have negligible effect on the resonance properties.

Computed results for the allowed cross section are illustrated, for various values of the parameters α_R, ϵ_0, E_M, g_c/g_1, and ω_0, in Figs. 6–9. The forbidden case counterparts are illustrated in Figs. 10 and 11. To facilitate various comparisons frequency scales in the figures have been adjusted such that in-resonances for various values are coincident, while out-resonances are not, in general.

The cross sections illustrated are indicative of the rich variety of resonance behavior anticipated in exciton-mediated RS. Among the general features of interest are the following: (a) differences for various cases in the relative intensity of $d\sigma/d\Omega$ in the regions immediately below E_1 and above $E_g + \omega_0$; (b) differences in the nature of the resonances and antiresonances in the various cases; (c) importance of the phonon frequency ω_0 in determining relative positions of incoming and out-

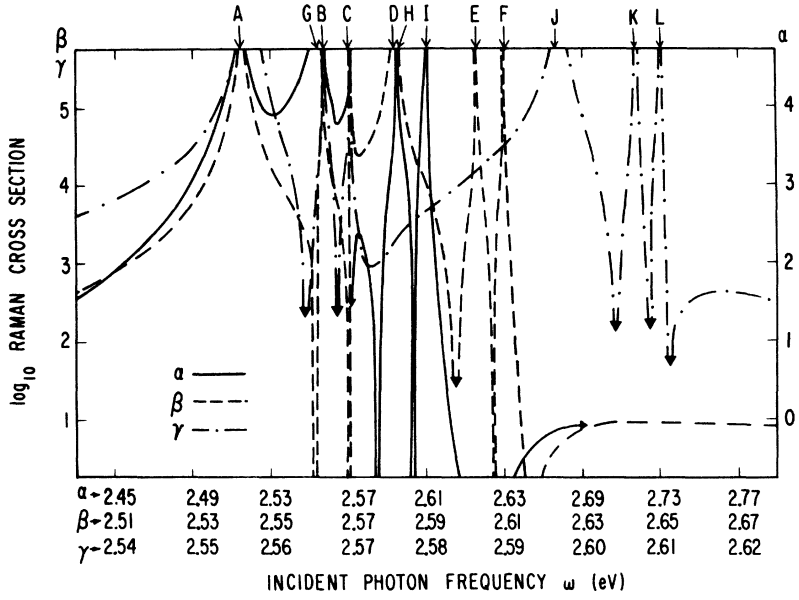

FIG. 8. Log_{10} of allowed cross section vs photon frequency ω for two values of ϵ_0. Dashed line: $\epsilon_0 = (\epsilon_0)_0$ (CdS value); solid line: $\epsilon_0 = 0.7(\epsilon_0)_0$; dashed-dot line: $\epsilon_0 = 1.5(\epsilon_0)_0$. A–F indicate the same points as in Fig. 7; G–I indicate $E_1 + \omega_0$ for $0.7\ (\epsilon_0)_0$; and J–L the same for $1.5(\epsilon_0)_0$. Omitted for clarity are two vertical solid lines indicating the $0.7(\epsilon_0)_0$ resonances at G and B.

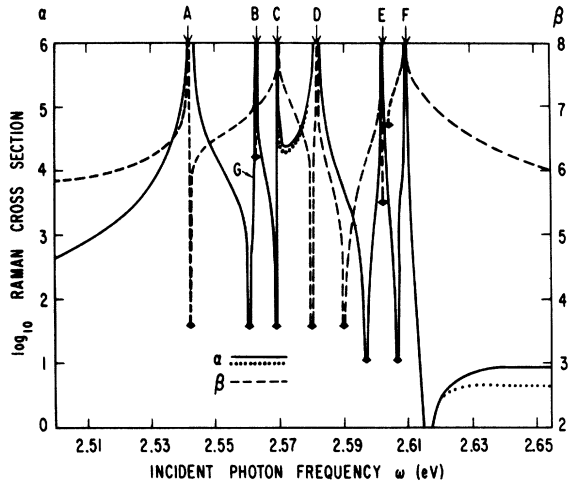

FIG. 9. Log_{10} of allowed cross section vs photon frequency ω for various values of g_c/g_1 and E_M. Solid line: $g_c/g_1 = (g_c/g_1)_0$, $E_M = (E_M)_0$ (CdS values); dashed line: $g_c/g_1 = 10(g_c/g_1)_0$. Dashed lines indicate departures from CdS results when $E_M = 10(E_M)_0$. A–F have the meanings specified in Fig. 7. A nearly vertical dashed line, omitted for clarity, should pass just to the right of point G.

going resonances, and, consequently, influencing interference behavior; (d) differences in sensitivity to variations in the parameters between the allowed and forbidden cases; and (e) the shifts in the discrete-state antiresonance frequencies due to continuum interference and the dependence of the strength of the antiresonances on the values of the parameters.

The most explicit demonstration of the effects of continuum dominance follows, of course, upon an increase in g_c/g_1, as illustrated in Figs. 9 and 12 for the allowed and forbidden cases, respectively. For the larger g_c/g_1 value in the allowed results, T_C simply overpowers T_D in the region above $E_g + \omega_0$, washing out antiresonant interference evident for CdS parameters. Likewise, a pronounced flattening out results in the forbidden case $d\sigma/d\Omega$. The continuum dominance leads to nearly similar intensities below E_1 and above $E_g + \omega_0$.

Similar behavior occurs in the purely hydrogenic model via variations in α_R or ϵ_0, as illustrated for α_R in the allowed case, for example, in Fig. 7. Large α_R corresponds to greater continuum dominance. However, regardless of how large α_R may be, T_D and T_C always interfere destructively above $E_g + \omega_0$, although the antiresonance is very narrow for very large α_R, as may be seen from the figure. As α_R decreases to CdS values, T_D/T_C increases correspondingly, so that broader antiresonant behavior results. If α_R were decreased sufficiently further, T_D would eventually overpower T_C, eliminating the antiresonance entirely. Similar behavior follows upon varying ϵ_0 (cf. Fig. 8). Forbidden case counterparts are illustrated in Figs. 11(b) and 12(b). Here the continuum dominance is so strong that α_R or ϵ_0 would have to be decreased by nearly an order of magnitude before interference effects comparable to those in the allowed case would be evident.

As for variations in E_M, in the allowed case the dominant contribution to T_C may be observed to

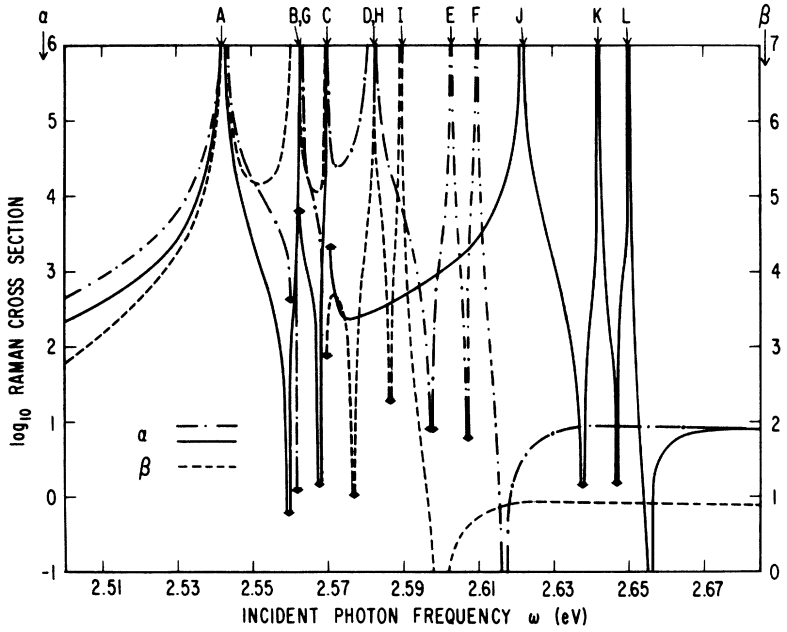

FIG. 10. Log_{10} of allowed cross section vs photon frequency ω for various values of ω_0. Dashed-dot line: $\omega_0 = (\omega_0)_0$ (CdS value); solid line: $\omega_0 = 2(\omega_0)_0$; dashed line: $\omega_0 = \frac{1}{2}(\omega_0)_0$. A–L indicate the same quantities as in Fig. 7, except for $(\omega_0)_0$, $\frac{1}{2}(\omega_0)_0$, and $2(\omega_0)_0$, respectively. Dashed-dot line to the left of C should be the leftmost line of a pair parallel and just to the right of the solid pair of lines near that point; these have been omitted for reasons of clarity. Also omitted at C is a nearly vertical dashed line.

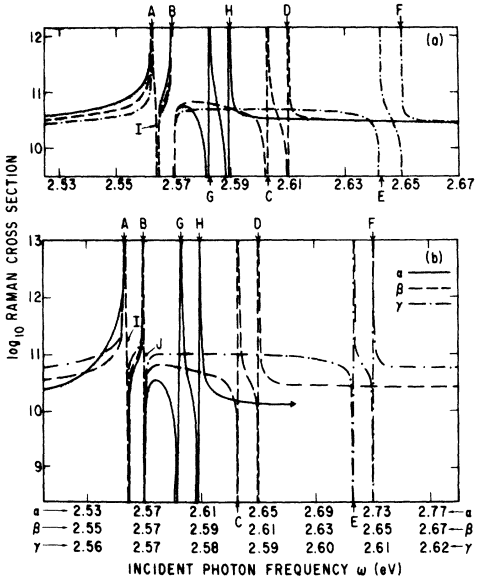

FIG. 11. Log_{10} of the forbidden cross section vs photon frequency ω. (a) Dependence on ω_0. Dashed line: $\omega_0=(\omega_0)_0$ (CdS values); solid line: $\omega_0=\frac{1}{2}(\omega_0)_0$; dashed-dot line: $\omega_0=2(\omega_0)_0$. *A*, *B* indicate E_2, E_g; *C*, *D* indicate these plus ω_0 for $(\omega_0)_0$; *E*, *F* the same for $2(\omega_0)_0$; and *G*, *H* the same for $\frac{1}{2}(\omega_0)$. Various lines omitted for clarity are vertical dashed-dot lines at *E* and *F*, solid and dashed-dot lines through *I*, and vertical lines of all three kinds at *B*. (b) Dependence on α_R. Dashed line: $\alpha_R=(\alpha_R)_0$ (CdS value); solid line: $\alpha_R=\frac{1}{2}(\alpha_R)_0$; dashed-dot line: $\alpha_R=2(\alpha_R)_0$. *A*–*H* indicate the same points as in (a), except for $(\alpha_R)_0$, $\frac{1}{2}(\alpha_R)_0$, and $2(\alpha_R)_0$, respectively. Omitted for clarity are nearly vertical solid and dashed-dot lines through both *I* and *J*.

come from values of η corresponding to $\frac{1}{2}\alpha_R\eta^2$ smaller than E_g, so that the cross section is relatively insensitive to increases in E_M from $2E_g$ (cf. Fig. 9). The extra power of $E_{\vec{\eta}}$ occurring in g_η for the forbidden case, however, implies that contributions from large $\vec{\eta}$ are relatively more important for this case than for the allowed. This increased sensitivity of $(d\sigma/d\Omega)_F$ to variations in E_M is evident from Fig. 12(a).

Variations in resonance behavior upon variation of ω_0, as illustrated in Figs. 10 and 11(a), result from changes in the relative disposition of the incoming and outgoing resonances, and from differences in the frequency dependence of T_C. The results illustrated are easily accounted for via the dependences discussed to this point.

Finally, we note the absence of complete destructive interference in between incoming resonances, for small α_R and ϵ_0 in the allowed case, due to the smallness of ω_0 relative to the interresonance spacings.

VI. DISCUSSION

In summary, we have derived, in the present work, polariton cross sections for forbidden- and quadrupole-exciton-mediated resonance RS, investigated the resonance properties within a hydrogenic model, and illustrated the theory via various numerical computations. We have also investigated the dependence of resonance properties on dielectric constant, exciton effective mass, exciton bandwidth, phonon frequency, continuum-to-discrete coupling ratio, and exciton damping. The results indicate that, in general, discrete exciton effects dominate the allowed cross section, while continuum effects dominate the forbidden one. Within a given category variation of the previously listed parameters may induce a wide variety of resonance behavior in $d\sigma/d\Omega$. For example, for certain values of the parameters, continuum-discrete interference above $E_g+\omega_0$ results in a broad antiresonance, which, however, may disappear entirely for other values of the parameters. In general,

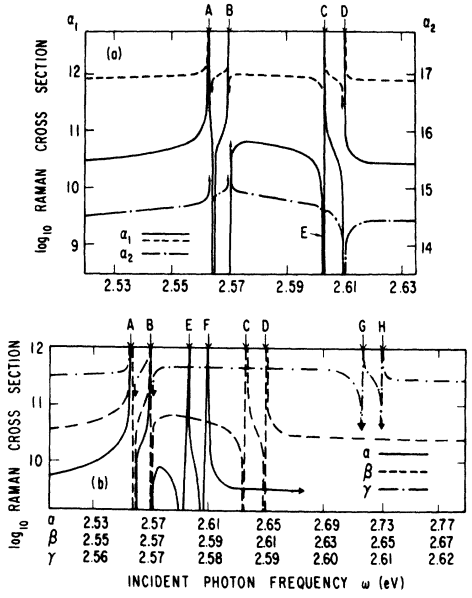

FIG. 12. Log_{10} of the forbidden cross section vs photon frequency ω. (a) Dependences on g_c/g_1 and E_M. Solid line: "CdS values"; dashed line: $E_M=10(E_M)_0$; dashed-dot line: $g_c/g_1=10(g_c/g_1)$. *A*–*D* indicate the same quantities as in Fig. 11. Omitted for clarity are vertical solid and dashed-dot lines, these nearly coincident with the dashed lines, at *A* and *B*. Also, at *E* the dashed-dot lines follow a nearly parallel pattern downward with the solid lines, being omitted for clarity. (b) Dependence on ϵ_0. Dashed line: $\epsilon_0=(\epsilon_0)_0$ (CdS value); solid line: $\epsilon_0=0.7(\epsilon_0)_0$; dashed-dot line: $\epsilon_0=1.5(\epsilon_0)_0$. *A*–*H* indicate the same points as in in Fig. 11(a), but for $(\epsilon_0)_0=0.7(\epsilon_0)_0$ and $1.5(\epsilon_0)_0$. Although only dashed lines are exhibited at *A* and *B* for clarity, the other lines follow nearly coincidently with these.

the different varieties of excitons discussed here may coexist within the same frequency region in a given material. The cross section may then be generalized appropriately, following the methods of the present treatment.

The differences in frequency dependence and resonance properties of $d\sigma/d\Omega$ in the various cases provide a possible means of identifying certain exciton or band properties (e.g., the symmetry character of the exciton envelope[9] and/or the band states involved). Analogous relationships have been pointed out, e.g., with regard to optical absorption by excitons.[9]

As of this time, RS data which is sufficiently detailed to allow a meaningful comparison with experiment of the differences predicted in the various cases does not seem to be available. Of course, various features of the dipole cross section, such as the resonance for $\omega \to E_1$, continuum domination below E_1, and the existence of "incoming" and "outgoing" resonances, have been experimentally verified[19] in a variety of materials, especially[13] II-VI compounds such as CdS and ZnSe. However, limited data on the relative intensities above E_g in CdS to those below E_1 exceed predicted values by about an order of magnitude.[15] Although the present work suggests a variety of ways in which increased intensities above E_g may arise, the data is not adequately detailed to allow singling out any one effect in particular.

Experimental results on TO-phonon scattering[13,20] demonstrate features which do not seem to be adequately accounted for by existing theory. Recently, dips below E_1 in TO scattering in CdS and Si were reported,[20] and interpreted as the result of cancellation between resonant and "nonresonant" terms (those arising from higher bands, e.g.). The suggestion has been made previously[21] that the relatively broad resonance behavior evident in TO as compared to LO scattering may be due to a dominance of continuum effects. In II it was shown, however, that variations in E_M and g_c/g_1, for dipole scattering in the present hydrogenlike model, could not adequately reproduce the reported behavior. If one examines the variations considered in the present paper as well, one finds that none of these can account properly for the observations. Thus interference due to terms with different signs in $g^{(3)}$, or originating from different bands, may indeed be the source of the observed behavior.

In conclusion, we are hopeful that the rich variety of resonance behavior predicted and illustrated in the present treatment will stimulate the detailed measurement of RS cross sections throughout the resonance regime. Such data will allow for extensive comparison of experiment with theory, and serve as well as a useful tool in studying crystalline properties.

ACKNOWLEDGMENTS

The author thanks Dr. J. L. Birman for his hospitality in arranging for the use of computer facilities at the Courant Institute, where certain of the present computations were carried out. Support for the latter by the U. S. Army Research Office (Durham) and the Aerospace Research Laboratories, Wright-Patterson Air Force Base (Dayton) are gratefully acknowledged.

APPENDIX: PHENOMENOLOGICAL THEORY OF DAMPED-POLARITON SCATTERING

The incorporation of damping effects in polariton scattering is of considerable interest, since exciton damping,[8] however small, is always present in semiconductors, and because inclusion of damping into the theory is expected to remove singular behavior predicted exactly at resonance in the dispersionless exciton model, in the absence of damping. Unfortunately, no satisfactory first-principles damped-polariton theory of exciton-mediated RS seems to have been advanced as yet. In this Appendix, we pursue the more modest goal of including damping phenomenologically into the energy-conserving RS1 cross section. Such a theory, we believe, allows one to draw qualitative conclusions regarding the influence of damping on the frequency dependence of $d\sigma/d\Omega$.

We begin by noting that our undamped cross section is similar in form to that of a free particle described by wave function $\psi \sim e^{i\vec{q}\cdot\vec{x}}$ scattering inelastically from $\vec{q} \to \vec{q}'$, namely,

$$d\sigma/d\Omega \propto (q'/q)\,|M(\vec{q},\vec{q}')|^2. \tag{A1}$$

In the presence of (exciton) damping, the polariton wave vector $\vec{q}$ becomes complex (cf. Ref. 22). We then interpret scattering as arising solely via the undamped portion of ψ, namely, $e^{i\,\mathrm{Re}(\vec{q})\cdot\vec{x}}$; as the beam traverses the crystal, however, it is now attenuated spatially with (vector) coefficient $2\,\mathrm{Im}(\vec{q})$. One can also show[23] that if all energy levels E_n damp similarly (i.e., damping functions Γ_n are all equal), then the modified equations of motion for the system may be obtained by replacing $\omega \to \omega + i\Gamma_n$ everywhere.[24] If one now employs the latter correspondence and the interpretation of $\mathrm{Re}(\vec{q})$ given above, then the cross section of Eq. (7) becomes, for the equal damping case,

$$\frac{d\sigma}{d\Omega} = (2\pi)^{-2}\,\frac{\mathrm{Re}(q)}{\mathrm{Re}(q')}\,|g^{(3)}|^2 \times |T_D(\omega \to \omega + i\Gamma) + T_C(\omega \to \omega + i\Gamma)|^2 . \tag{A2}$$

This result describes scattering due to the unattenuated portions of the polariton beams. When relating a specific experiment to the theory, of

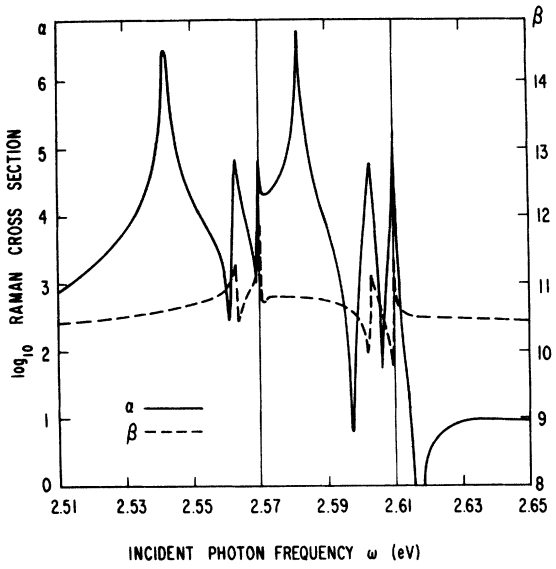

FIG. 13. Log_{10} Raman cross section vs photon frequency ω, in the presence of damping. Solid line: allowed; dashed line: forbidden. CdS parameters are employed. Discrete state Γ is taken as 0.0005, while $\Gamma \to +0$ is employed for the continuum. Peaks associated with E_i and $E_i + \omega_0$ are evident (cf. Fig. 4).

course, attenuation of the incoming and outgoing beams, with coefficients $\propto \text{Im}\vec{q}, \vec{q}'$, need be accounted for[25] as well.

We now present numerical computations based on Eq. (A2). For simplicity, we employ $\lim \Gamma \to +0$ in the continuum contributions[26] to T_C, q, and q'. The typical value $\Gamma = 0.0005$ eV is employed[27] in the discrete-state contributions. The results (CdS parameters) are illustrated, for allowed and forbidden cases, in Fig. 13. The singularities and vanishings of $d\sigma/d\Omega$ which were evident in the absence of damping are now continuously rounded out, and "reflection gaps"[22] filled in. In order for the relative heights of the various peaks to be of significance, the $\Gamma_n(\omega)$ need to be chosen carefully, possibly being deduced from optical absorption data.

The present treatment has demonstrated the "rounding-out" effect expected in the energy-conserving cross section in the presence of damping. One observes, however, that undamped theory does yield accurate predictions nearly everywhere except in frequency regions of the order of the Γ_n about the various resonance and antiresonance frequencies. These modifications being borne in mind, one is able to properly interpret the various undamped results presented throughout the text.

*Supported by the Office of Naval Research under Grant No. NONR-N00014-69-A-0200-6206, the National Science Foundation Grant No. GP-10943, and the Air Force Office of Scientific Research Grant No. AFOSR 610-67.

[1]B. Bendow and J. L. Birman, in *Light Scattering Spectra of Solids*, edited by G. B. Wright (Springer-Verlag, New York, 1969); E. Burstein, D. L. Mills, A. Pinczuk, and S. Ushioda, Phys. Rev. Letters 22, 348 (1969); B. Bendow, Ph. D. thesis (New York University, 1969) (unpublished); D. L. Mills and E. Burstein, Phys. Rev. 188, 1465 (1969), and references given in the above.

[2]B. Bendow and J. L. Birman, Phys. Rev. B 1, 1678 (1970).

[3]B. Bendow, Phys. Rev. B 2, 5051 (1970).

[4]U. Fano, Phys. Rev. 103, 1202 (1956); J. J. Hopfield, *ibid.* 112, 1555 (1958).

[5]See, for example, R. J. Elliot, Phys. Rev. 108, 1384 (1957); E. J. Johnson, in *Semiconductors and Semimetals*, edited by R. K. Willardson and A. C. Beer (Academic, New York, 1967), Vol. III, and references therein.

[6]A. K. Ganguly and J. L. Birman, Phys. Rev. 162, 806 (1967).

[7]D. Mills and E. Burstein, Phys. Rev. 188, 1465 (1969); and Ref. 3.

[8]R. S. Knox, *Theory of Excitons* (Academic, New York, 1963).

[9]R. J. Elliot, Phys. Rev. 108, 1384 (1957).

[10]J. O. Dimmock, in *Semiconductors and Semimetals*, edited by R. K. Willardson and A. C. Beer (Academic, New York, 1967), Vol. III.

[11]R. S. Knox, Ref. 8, Chap. 4.

[12]Cf., e.g., B. Bendow, Ph. D. thesis (New York University, 1969) (unpublished).

[13]R. C. Leite and J. F. Scott, in *Light Scattering Spectra of Solids*, edited by G. B. Wright (Springer-Verlag, New York, 1969).

[14]J. J. Hopfield, Phys. Rev. 182, 945 (1969).

[15]B. Bendow, J. L. Birman, A. K. Ganguly, R. C. Leite, J. F. Scott, and T. C. Damen, Opt. Commun. 1, 267 (1970).

[16]In the various computations throughout the paper we will employ a somewhat arbitrarily chosen standard set of parameters, which will be referred to as "CdS parameters." The values employed are approximately appropriate to the *A* exciton in CdS. We do *not* mean to imply, however, that a given physical situation (such as forbidden or quadrupole transitions) necessarily exists in CdS; the values are chosen merely for reasons of convenience, familiarity, and standardization.

[17]R. S. Knox, Ref. 8, Chap. 9.

[18]R. Loudon, Proc. Roy. Soc. (London) A275, 218 (1963).

[19]R. C. Leite and S. P. Porto, Phys. Rev. Letters 17, 10 (1966); R. C. Leite, J. F. Scott, and T. C. Damen, *ibid.* 22, 780 (1969); M. V. Klein and S. P. Porto, *ibid.* 22, 782 (1969); R. C. Leite, J. F. Scott, and T. C. Damen, Phys. Rev. 188, 1285 (1969); and Ref. 13. Some experimental observations of forbidden and quadrupole scattering have recently been reported by R. M. Martin and T. C. Damen [Phys. Rev. Letters 26, 86 (1971)] and by S. P. Porto *et al.* (private communication).

[20]J. M. Ralston, R. L. Wadsack, and R. K. Chang, Phys. Rev. Letters 25, 814 (1970).

[21]D. Mills and E. Burstein, Phys. Rev. 188, 1465 (1969).

[22]M. Born and K. Huang, *Dynamical Theory of Crystal*

Lattices (Oxford U. P., Oxford, England, 1956), Chap. II.

[23]B. Bendow, Ph.D. thesis (New York University, 1969) (unpublished).

[24]We have omitted, for simplicity, the real energy shift Δ_n, which may be reabsorbed into the previously defined energy levels E_n.

[25]See, for example, R. Loudon, J. Phys. (Paris) 26, 667 (1965); and B. Bendow, Ph.D thesis (New York University, 1969) (unpublished).

[26]Actually, for $\Gamma \to 0$ the real part of T_C becomes infinite *exactly* at E_g and $E_g + \omega_0$; however, this behavior does not substantially affect any other frequency values, and may be removed by any nonzero choice.

[27]This value for Γ is approximately the one found to best fit reflectivity data in CdS by J. J. Sein [Ph. D. thesis (New York University, 1969) (unpublished)].

PHYSICAL REVIEW B VOLUME 4, NUMBER 2 15 JULY 1971

M-Center Fluorescence in NaCl and KI Crystals

R. W. Dreyfus

IBM Thomas J. Watson Research Center, Yorktown Heights, New York 10598

(Received 15 March 1971)

The first excited singlet state Σ_u^+ of the *M* center fluoresces in the near infrared. This fluorescence has been observed at low temperatures and the decay time found to be 41 nsec for NaCl and 60 nsec for KI. In KI, a maximum time (5 nsec) is established for filling the Σ_u^+ state from a higher-excited state Π_u. In addition, the fluorescence spectrum of the *M* center in KI is reported for the first time. At ~10 °K, the fluorescence intensity peaks at 0.818 eV = 1.52 μ and has a half-width of 0.100 eV.

I. INTRODUCTION

The *M* center consists of two *F* centers on adjacent anion sites and is analogous to the hydrogen molecule.[1,2] The analogy arises because this center is composed of two electrons bound to two anion vacancies which act as positive charges. Because of this similarity, the electronic energy states are identified by molecular terminology.[1] The lowest four singlet states are shown in Fig. 1; triplet states do not enter into the present discussion.

The primary purpose of the present experiment is to determine the time constants for fluorescent decay from the excited states shown in Fig. 1. Specifically, the following quantities are sought: the wavelengths and time constants (τ_1) for the $\Sigma_u^+ \to \Sigma_g^+$ transition in NaCl and KI, and the time (τ_2) for the $\Pi_u \to \Sigma_u^+$ transition. Previous work has not indicated a higher-energy emission line due to a direct $\Pi_u \to \Sigma_g^+$ (ground state) deexcitation in other alkali halides.

The above transition times are directly observable since a *Q*-switched ruby laser excites the *M* centers quasi-instantaneously. The ruby photons have an energy of 1.79 eV (6943 Å). This energy falls in the *M* band in NaCl and the M_F band in KI[1,3]; Fig. 1 shows the states involved in these absorption bands. Thus the ruby laser excites the *M* centers to the Σ_u^+ and Π_u states in the respective crystals. The measurement consists of observing the fluorescent intensity due to the $\Sigma_u^+ \to \Sigma_g^+$ transition as a function of time after the ruby laser flash. The dynamics of filling and emptying the Σ_u^+ state are then determined from the time dependence of this transition.

II. EXPERIMENTAL METHOD

M centers were formed in crystals which had previously been colored[4] so as to have an *F*-center concentration up to 2×10^{17} cm^{-3}. In order to avoid large clusters of *F* centers, the crystals were cooled rapidly from high temperature to 80 °K. The KI crystals were quenched within the optical Dewar; the crystals were first heated to 400 °C

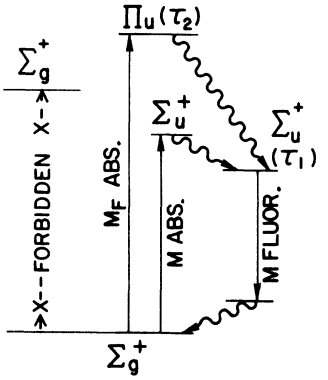

FIG. 1. Energy levels of the *M* center as given by molecular-spectroscopic terms. This is equivalent to considering the *M* center as a hydrogenlike molecule immersed in an isotropic dielectric. It is understood that the right-hand Σ_u^+ level is derived from the upper Σ_u^+ state by the usual rapid Franck-Condon shift (to lower energies on a configuration coordinate diagram); see Fig. 43 of Ref. 1(c). The time constants for deexcitation from the upper levels are given in parentheses.